Published in "Nature Geoscience 12(3): 168–173, 2019" which should be cited to refer to this work.

A consensus estimate for the ice thickness distribution of all glaciers on Earth

Daniel Farinotti[1,2*], Matthias Huss[1,3], Johannes J. Fürst[4], Johannes Landmann[1,2], Horst Machguth[3,5], Fabien Maussion[6] and Ankur Pandit[7,8]

Knowledge of the ice thickness distribution of the world's glaciers is a fundamental prerequisite for a range of studies. Projections of future glacier change, estimates of the available freshwater resources or assessments of potential sea-level rise all need glacier ice thickness to be accurately constrained. Previous estimates of global glacier volumes are mostly based on scaling relations between glacier area and volume, and only one study provides global-scale information on the ice thickness distribution of individual glaciers. Here we use an ensemble of up to five models to provide a consensus estimate for the ice thickness distribution of all the about 215,000 glaciers outside the Greenland and Antarctic ice sheets. The models use principles of ice flow dynamics to invert for ice thickness from surface characteristics. We find a total volume of $158 \pm 41 \times 10^3$ km^3, which is equivalent to 0.32 ± 0.08 m of sea-level change when the fraction of ice located below present-day sea level (roughly 15%) is subtracted. Our results indicate that High Mountain Asia hosts about 27% less glacier ice than previously suggested, and imply that the timing by which the region is expected to lose half of its present-day glacier area has to be moved forward by about one decade.

Glaciers and ice caps outside the Greenland and Antarctic ice sheets ('glaciers' in the following) are changing rapidly in response to climate change[1]. Although they only contain a fraction of the worldwide ice volume[2], the consequences of their mass loss are widespread and of global significance: glacier changes affect global trends in freshwater availability[3,4], have dominated cryospheric contributions to recent sea level changes[5,6] and are anticipated to affect regional water resources over the twenty-first century[7,8]. Clearly, projections of such impacts require an estimate of the ice volume stored within present-day glaciers, and for regional- to local-scale projections the ice thickness distribution can also be essential[9,10]. Recent studies showed that even small features in the bedrock topography can cause decadal-scale variations in both ice dynamics response[11] and subglacial water discharge[12].

Despite far-reaching implications, knowledge of the ice thickness distributions of the world's glaciers is remarkably limited. The Glacier Thickness Database (GlaThiDa), which centralizes ice thickness measurements outside the two ice sheets, presently contains information for only about 1,000 out of the 215,000 glaciers worldwide[13]. This is despite important advances in the instrumentation used to measure ice thickness[14,15], with airborne platforms now capable of operating in mountainous environments as well[16].

Owing to the lack of direct measurements, relations between glacier area and ice volume[17] have traditionally been used to estimate global glacier volumes[18–21]. For individual glaciers, instead, a suite of methods that infer the spatial ice thickness distribution from surface characteristics have been proposed[22–27]. Such methods use topographical information—typically extracted from digital elevation models (DEMs)—to estimate the distribution of the glacier's surface mass balance and, hence, its mass turnover. The latter is then inverted for ice thickness by using principles of ice flow dynamics. Regional-scale estimates based on such methods have been presented[7,28,29], but only one estimate exists at the global scale[30]. This seems unfortunate in light of the results of the recent ice thickness models intercomparison experiment (ITMIX)[31], which showed how individual models can suffer from substantial uncertainties, and that pooling the results from different models significantly increases the estimate's robustness and accuracy.

Here we take advantage of the ITMIX findings and use a combination of up to five ice thickness estimation models[29,30,32–34] (Fig. 1) to provide an ensemble-based estimate for the ice thickness distribution of each of the about 215,000 glaciers included in the Randolph Glacier Inventory (RGI) version 6.0 (ref. [35]). All the models use the glacier's surface topography, obtained from different DEM sources, and principles of ice flow dynamics to invert for local ice thickness (Methods and Supplementary Section 1). Model performance is assessed against observations in a cross-validation scheme (Methods and Supplementary Fig. 1), and inverse variance and bias weighting (Methods and Supplementary Table 1) are used to produce a consensus composite result. Subtraction of the so-obtained ice thickness distribution from the surface provides a corresponding bedrock topography.

Distribution of global ice volume

The regional distribution of the global glacier ice volume, which includes the share located below present sea level, is given in Fig. 2. Based on the composite solution, we estimate a global glacier volume of $158 \pm 41 \times 10^3$ km^3 (Table 1). This corresponds to a potential sea level contribution of 0.32 ± 0.08 m when the volume already

[1]Laboratory of Hydraulics, Hydrology and Glaciology (VAW), ETH Zurich, Zurich, Switzerland. [2]Swiss Federal Institute for Forest, Snow and Landscape Research (WSL), Birmensdorf, Switzerland. [3]Department of Geosciences, University of Fribourg, Fribourg, Switzerland. [4]Institute of Geography, Friedrich-Alexander-University Erlangen-Nuremberg (FAU), Erlangen, Germany. [5]Department of Geography, University of Zurich, Zurich, Switzerland. [6]Institute of Atmospheric and Cryospheric Sciences, University of Innsbruck, Innsbruck, Austria. [7]Interdisciplinary Programme in Climate Studies, Indian Institute of Technology Bombay, Mumbai, India. [8]Hydro-Remote Sensing Applications (H-RSA) Group, Department of Civil Engineering, Indian Institute of Technology Bombay, Mumbai, India. *e-mail: daniel.farinotti@ethz.ch

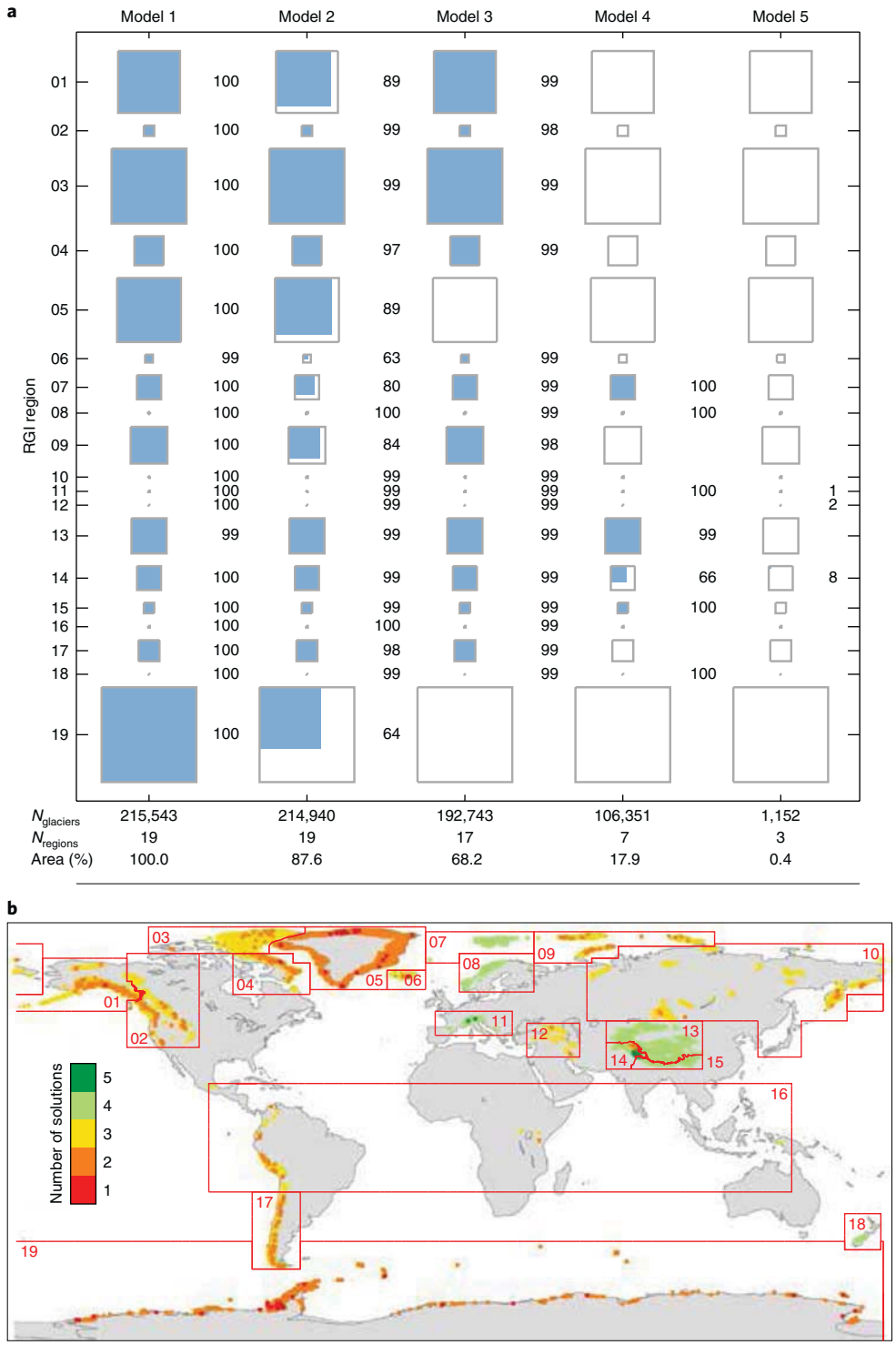

Fig. 1 | Overview of individual model contributions. a, Total glacier area (squares) for every RGI region (panel **b** and Table 1 give the region keys), together with the area portion (%) considered by each model (blue). For each model, the total number of considered glaciers ($N_{glaciers}$) and regions ($N_{regions}$) is provided, together with the share of total area (%) considered. **b**, Number of model solutions available for every glacier. Model 1, Huss and Farinotti[30]; Model 2, Frey et al.[29]; Model 3, Maussion et al.[33]; Model 4, Fürst et al.[32]; Model 5, Ramsankaran et al.[34].

located below sea level at present ($23.9 \pm 6.2 \times 10^3$ km^3, or about 15% of the total) is subtracted. The largest glacier volumes are found in the Arctic ($74.7 \pm 19.4 \times 10^3$ km^3 (47.3% of the global volume) when combining the Canadian and Russian Arctic, Greenland's periphery and Svalbard) and in the Antarctic periphery ($46.5 \pm 12.1 \times 10^3$ km^3 (29.4%)). After Alaska ($19.0 \pm 4.9 \times 10^3$ km^3 (12.0%)), High Mountain Asia—which consists of South and Central Asia—is the area with the largest ice volume ($7.0 \pm 1.8 \times 10^3$ km^3 (4.4%)) outside the polar regions. Combined, the remaining nine regions only contain about 6.9% ($11.0 \pm 2.8 \times 10^3$ km^3) of the global ice volume.

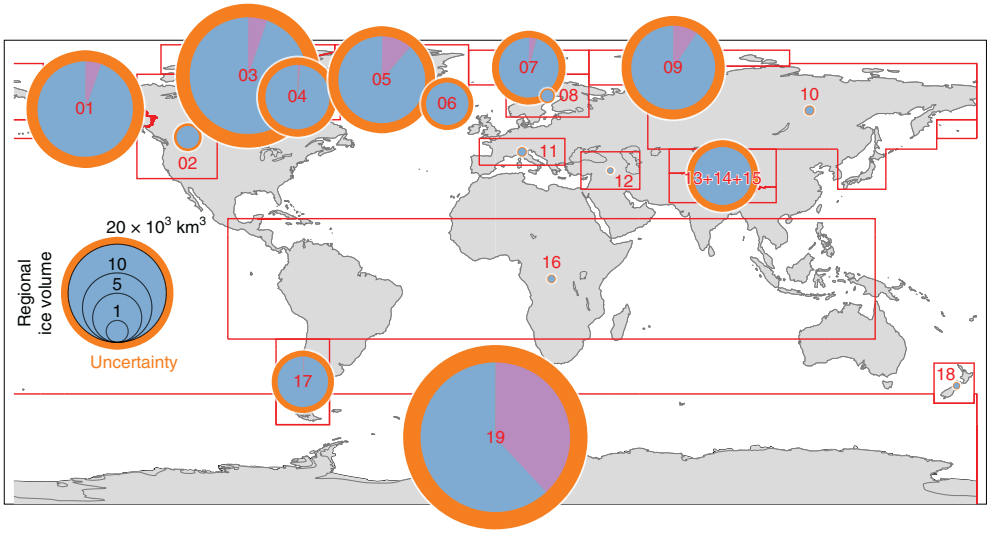

Fig. 2 | Regional distribution of the calculated glacier ice volume. The pie charts are centred over the considered RGI region (red labels and lines). The pie area is proportional to the calculated ice volume (Table 1) and discerns between the ice above (blue) and below (violet) present-day sea level. The outer ring (orange) reflects the estimated uncertainty (Methods).

Table 1 | Regionally aggregated summary statistics for the provided results

RGI region	*N*	*A* (km²)	*V* (10³ km³)	$\bar{h}$ (m)	SLE (mm)	BSL (%)
01 Alaska	27,108	86,677	18.98 ± 4.92	218	43.3 ± 11.2	5.4
02 Western Canada and United States	18,862	14,629	1.06 ± 0.27	72	2.6 ± 0.7	0.0
03 Arctic Canada North	4,549	104,920	28.33 ± 7.35	270	64.8 ± 16.8	5.3
04 Arctic Canada South	7,422	40,860	8.61 ± 2.23	210	20.5 ± 5.3	1.3
05 Greenland periphery	19,306	89,651	15.69 ± 4.07	175	33.6 ± 8.7	11.3
06 Iceland	567	11,052	3.77 ± 0.98	341	9.1 ± 2.4	0.2
07 Svalbard	1,615	33,932	7.47 ± 1.94	220	17.3 ± 4.5	4.1
08 Scandinavia	3,417	2,947	0.30 ± 0.08	101	0.7 ± 0.2	0.0
09 Russian Arctic	1,069	51,551	14.64 ± 3.80	283	32.0 ± 8.3	9.5
10 North Asia	5,144	2,399	0.14 ± 0.04	56	0.3 ± 0.1	0.0
11 Central Europe	3,927	2,091	0.13 ± 0.03	61	0.3 ± 0.1	0.0
12 Caucasus and Middle East	1,887	1,305	0.06 ± 0.02	48	0.2 ± 0.0	0.0
13 Central Asia	54,429	49,295	3.27 ± 0.85	66	7.9 ± 2.0	0.0
14 South Asia West	27,986	33,561	2.87 ± 0.74	85	6.9 ± 1.8	0.0
15 South Asia East	13,119	14,734	0.88 ± 0.23	59	2.1 ± 0.5	0.0
16 Low latitudes	2,940	2,341	0.10 ± 0.03	42	0.2 ± 0.1	0.0
17 Southern Andes	15,908	29,368	5.34 ± 1.39	181	12.8 ± 3.3	0.7
18 New Zealand	3,537	1,161	0.07 ± 0.02	63	0.2 ± 0.0	0.0
19 Antarctic and subantarctic[a]	2,751	132,771	46.47 ± 12.06	349	69.4 ± 18.0	38.1
Total	215,543	705,253	158.17 ± 41.03	224	324.3 ± 84.1	15.1

[a]As the Antarctic ice sheet is not included in this region, we refer to it as to the Antarctic periphery throughout the manuscript. The number of considered glaciers (*N*) and their area (*A*) is given together with the regional glacier volume (*V*) and the corresponding average ice thickness ($\bar{h}$). The potential sea-level equivalent (SLE) accounts for the ice portion presently located below sea level (BSL). All numbers refer to the composite solution.

Significant ice volumes located below the present sea level, which would not contribute to future sea-level rise even if melted, are found in the Antarctic periphery (38% of the regional volume), Greenland periphery (11%), Russian Arctic (9.5%), Alaska (5.4%), and northern Arctic Canada (5.3%). In all cases, the relatively large percentages are indicative for the deeply incised fjord systems that characterize ocean-terminating glaciers in the polar regions[36].

Our estimate of the global glacier volume is about 18% lower than the average of previous estimates (Supplementary Table 2), but relatively close (difference of −7.1%) to that reported by Huss and Farinotti[30]. The latter study—referred to as HF12 in the following—is the only one to provide global-scale estimates for the ice thickness distribution of individual glaciers so far. Although our total ice volume agrees with that of HF12, the regional distributions differ substantially (Fig. 3). The most important difference is found in the Antarctic periphery, where our estimate is 24% higher, and is now close to the average of previous studies (Supplementary Table 2). The higher estimate is compensated by reduced ice volumes

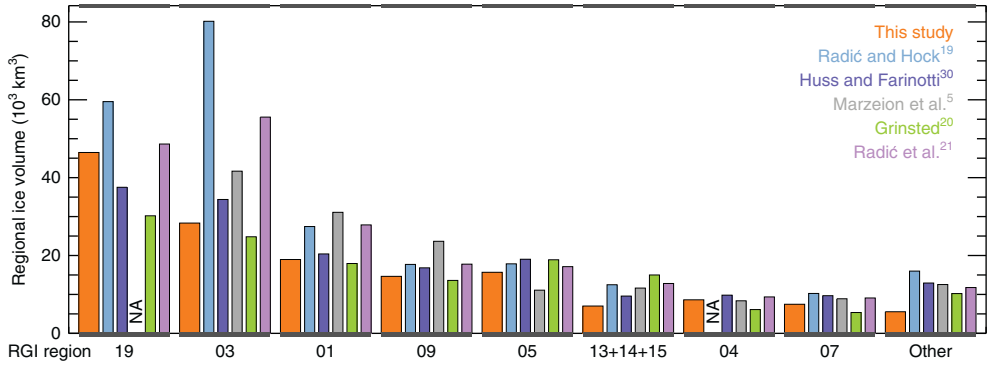

Fig. 3 | Overview of individual model contributions. NA indicates that a corresponding estimate was not available. Region labels follow those in Fig. 1 and Table 1.

obtained for the Arctic (−17% compared to HF12), High Mountain Asia (−27%) and other regions, specifically including the Southern Andes (−20%). When compared to the average of previous studies, the most striking difference is found for High Mountain Asia, where our results indicate a 46% lower total ice volume (Supplementary Table 2). The fraction of global ice volume located below present-day sea level is very close (within ±2.5%) to a previous estimate[37] that was based on order-of-magnitude considerations.

Implications for glacier evolution, and ice discharge

The implications of the revised estimates, and the potential insights they provide, are demonstrated for the two regions in which the estimated total glacier volume has changed the most in comparison to HF12: High Mountain Asia and the Antarctic periphery.

For High Mountain Asia, we used the Global Glacier Evolution Model (GloGEM)[10] to provide projections for the glacier evolution until 2100 (Methods). Keeping the model forcing and parameters unaltered but adjusting the initial ice thickness distribution of the simulations causes significant differences in the evolution of both the glacierized area and expected glacier runoff. Simulations performed by using the HF12 ice thickness (Simulation 1), for example, suggest that the region's glacier area (roughly 97,000 km^2 according to the RGI) is likely to have shrunk by 50% by the late 2070s. Replacing the initial ice thickness distribution of the about 96,000 glaciers in the region with the here-presented results and repeating the simulations (Simulation 2) moves this point in time forward to the mid 2060s (Supplementary Fig. 2). The effect of a changed initial ice thickness distribution is noticeable in the projected future glacier water discharge as well (Supplementary Fig. 3). Simulation 1, for example, indicates that the average July–August runoff from the presently glacierized surfaces across High Mountain Asia could be reduced by roughly 15% by the 2090s when compared to present levels. In Simulation 2, this figure changes to a reduction by 24%, which corresponds to an additional July–August runoff decrease of 6×10^9 m^3 month^{-1}. In light of the importance of glacier melt for the regional water supply[3,8,38], these differences are unsettling, and call for a better characterization of the regional glacier ice volume. At the moment, the latter is hampered by the paucity of available in situ measurements, and is reflected in the large spread between results provided by individual models (Supplementary Fig. 4).

For the Antarctic periphery, we calculated the amount of ice discharged across the calving front of all ocean-terminating glaciers contained in the RGI. We did so by intersecting our distributed ice thickness estimates with observed ice flow velocities (Methods). The resulting total ice flux is 43 ± 8 Gt a^{-1}, equivalent to about 3% of the calving flux from the entire Antarctic ice sheet[39]. This quantity is of relevance because the non-floating portion of the discharged ice directly contributes to sea-level change. The subglacial topography of glaciers in the Antarctic periphery is also of interest in light of the highly dynamic response observed for outlet glaciers after the loss of floating tongues and ice shelves[40]. This response, which can result in a manifold acceleration in ice flow velocities[40], is recognized to be decisively modulated by the buttressing induced by local topography, including subglacial features[41]. Despite still being affected by considerable uncertainties (see the next section), the here-presented ice thickness estimates provide a better basis on which such dynamic responses can be estimated.

Causes of discrepancies, uncertainties and way forward

We attribute a large part of the differences with respect to HF12 to the way that individual glaciers are represented in the inventory that is at the base of our analysis. On the one hand, the quality and completeness of RGI version 6.0 has substantially improved compared to that of version 2.0, which was used in the earlier study. On the other hand, many glacier complexes are separated into individual units in the new inventory[35]. These differences are best reflected in the reported total number of glaciers and area, with roughly 44,500 additional entries (+26%) in version 6.0 compared to version 2.0 despite a minor change (−4%) in the total area. Although the addition of formerly disregarded, mostly small, glaciers is unlikely to affect the estimated regional volumes significantly, the failure to separate glacier complexes is known to introduce biases towards higher ice thicknesses, because a clear relation exists between glacier area and volume. We suggest that the above changes (Supplementary Fig. 5 gives an illustrative example) particularly affected the estimates for High Mountain Asia, with the newer inventory discerning almost 30,000 additional glaciers (+44%) but reporting a 19% smaller total area. For that region, our total volume estimate now lies even below the lowest one reported in Frey et al.[29].

For the Antarctic periphery, we attribute the large differences with respect to HF12 to the DEMs used to represent the glacier surfaces (Methods). Although HF12 exclusively used data from the Advanced Spaceborne Thermal Emission and Reflection Radiometer (ASTER) DEM[42] (known to be noisy for some parts of the Antarctic), here we use data from the much-improved Radarsat Antarctic Mapping Project (RAMP[43]). The smoother surfaces of the latter product cause local surface slopes to be smaller, which in turn results in larger ice thicknesses due to the inverse relation to ice flow driving stress[31].

The significant differences between regional estimates provided by various studies (Fig. 3) and models (Supplementary Fig. 4) is a clear indication that the present estimates still suffer from significant uncertainties. Two main sources can be discerned in this respect: the uncertainty in the models used to estimate the ice thickness, and the uncertainty in the driving input data. Although the first uncertainty can be reasonably quantified (Methods) and can be

reduced by combining the results of different approaches[31], ample room for model improvement still exists. This is particularly evident when considering point-by-point comparisons between measured and modelled ice thicknesses: although the mean thickness is usually well captured (Supplementary Fig. 1) and no bias with respect to glacier size can be discerned (Supplementary Fig. 2), all the models regularly show local deviations of up to twice the observed mean ice thickness. This is not least related to the ill-posed nature of the ice-thickness-inversion problem. As outlined by Bahr et al.[44], inverting the surface characteristics for ice thickness can create a calculation instability that grows exponentially with glacier size, and random errors from this instability can overwhelm other sources of uncertainty. Although (1) our ensemble approach minimizes the influence of random errors and (2) the ill-posed nature of the problem is taken into account through spatial smoothing of individual model outputs, such limitations have to be kept in mind when using the results for analyses that are potentially sensitive to small-scale topography.

Ways to further improve the model performance—which include the assimilation of additional surface information such as ice flow velocities, anticipated to soon become available at the global scale—have been sketched previously[31]. To improve the consistency and completeness of global data sets for glacier outlines, surface elevation models and measured ice thickness would, however, be of equal importance to further improve the reliability of regional-scale estimates. Individual, dedicated campaigns in particularly data-scarce regions could prove efficient towards this target, provided that the results are made openly available.

For the time being, the results presented here provide a consensus estimate of the ice thickness distribution of all the glaciers on Earth outside the polar ice sheets. The results are anticipated to have implications ranging from projected sea-level change rates to estimated future water availability. The results can be retrieved from https://doi.org/10.3929/ethz-b-000315707.

References

1. Vaughan, D. et al. in *Climate Change 2013: The Physical Science Basis* (eds Stocker, T. F. et al.) 317–382 (IPCC, Cambridge Univ. Press, 2013).
2. Lambeck, K., Rouby, H., Purcell, A., Sun, Y. & Sambridge, M. Sea level and global ice volumes from the Last Glacial Maximum to the Holocene. *Proc. Natl Acad. Sci. USA* **111**, 15296–15303 (2014).
3. Kaser, G., Großhauser, M. & Marzeion, B. Contribution potential of glaciers to water availability in different climate regimes. *Proc. Natl Acad. Sci. USA* **107**, 20223–20227 (2010).
4. Rodell, M. et al. Emerging trends in global freshwater availability. *Nature* **557**, 651–659 (2018).
5. Marzeion, B., Jarosch, A. & Hofer, M. Past and future sea-level change from the surface mass balance of glaciers. *Cryosphere* **6**, 1295–1322 (2012).
6. Church, J. et al. in *Climate Change 2013: The Physical Science Basis* (eds Stocker, T. et al.) 1137–1216 (IPCC, Cambridge Univ. Press, 2013).
7. Kraaijenbrink, P., Lutz, A., Bierkens, M. & Immerzeel, W. Impact of a 1.5°C global temperature rise on the glaciers of High Mountain Asia. *Nature* **549**, 257–260 (2017).
8. Huss, M. & Hock, R. Global-scale hydrological response to future glacier mass loss. *Nat. Clim. Change* **8**, 135–140 (2018).
9. Gabbi, J., Farinotti, D., Bauder, A. & Maurer, H. Ice volume distribution and implications on runoff projections in a glacierized catchment. *Hydrol. Earth Syst. Sci.* **16**, 4543–4556 (2012).
10. Huss, M. & Hock, R. A new model for global glacier change and sea-level rise. *Front. Earth Sci.* **3**, 54 (2015).
11. Nias, I., Cornford, S. & Payne, A. New mass conserving bedrock topography for Pine Island Glacier impacts simulated decadal rates of mass loss. *Geophys. Res. Lett.* **45**, 3173–3181 (2018).
12. Amundson, J. & Carroll, D. Effect of topography on subglacial discharge and submarine melting during tidewater glacier retreat. *J. Geophys. Res. Earth Surf.* **123**, 66–79 (2017).
13. Gärtner-Roer, I. et al. *Glacier Thickness Database 2.0* (World Glacier Monitoring Service, 2016); https://doi.org/10.5904/wgms-glathida-2016-07
14. Allen, C. *IceBridge MCoRDS L2 Ice Thickness* (NASA DAAC at the National Snow and Ice Data Center, 2010).
15. Zamora, R., Uribe, J., Oberreuter, J. & Rivera, A. Ice thickness surveys of the southern Patagonian ice field using a low frequency ice penetrating radar system. In *First IEEE Inter. Symp. Geosci. Remote Sensing (GRSS-CHILE)* 1–4 (IEEE, 2017).
16. Rutishauser, A., Maurer, H. & Bauder, A. Helicopter-borne ground-penetrating radar investigations on temperate alpine glaciers: a comparison of different systems and their abilities for bedrock mapping. *Geophysics* **81**, WA119 (2016).
17. Bahr, D. B., Pfeffer, W. T. & Kaser, G. A review of volume-area scaling of glaciers. *Rev. Geophys.* **53**, 95–140 (2015).
18. Dyurgerov, M. & Meier, M. *Glaciers and the Changing Earth System: A 2004 Snapshot* Institute of Arctic and Alpine Research Occasional Paper 58 (Univ. Colorado, 2005).
19. Radić, V. & Hock, R. Regional and global volumes of glaciers derived from statistical upscaling of glacier inventory data. *J. Geophys. Res.* **115**, F01010 (2010).
20. Grinsted, A. An estimate of global glacier volume. *Cryosphere* **7**, 141–151 (2013).
21. Radić, V. et al. Regional and global projections of twenty-first century glacier mass changes in response to climate scenarios from global climate models. *Clim. Dyn.* **42**, 37–58 (2014).
22. Farinotti, D., Huss, M., Bauder, A., Funk, M. & Truffer, M. A method to estimate ice volume and ice thickness distribution of alpine glaciers. *J. Glaciol.* **55**, 422–430 (2009).
23. Morlighem, M. et al. A mass conservation approach for mapping glacier ice thickness. *Geophys. Res. Lett.* **38**, L19503 (2011).
24. Linsbauer, A., Paul, F. & Haeberli, W. Modeling glacier thickness distribution and bed topography over entire mountain ranges with GlabTop: application of a fast and robust approach. *J. Geophys. Res.* **117**, F03007 (2012).
25. McNabb, R. et al. Using surface velocities to calculate ice thickness and bed topography: a case study at Columbia Glacier, Alaska. *J. Glaciol.* **58**, 1151–1164 (2012).
26. van Pelt, W. J. J. et al. An iterative inverse method to estimate basal topography and initialize ice flow models. *Cryosphere* **7**, 987–1006 (2013).
27. Brinkerhoff, D. J., Aschwanden, A. & Truffer, M. Bayesian inference of subglacial topography using mass conservation. *Front. Earth Sci.* **4**, 1–15 (2016).
28. Clarke, G. K. C. et al. Ice volume and subglacial topography for western Canadian glaciers from mass balance fields, thinning rates, and a bed stress model. *J. Clim.* **26**, 4282–4430 (2013).
29. Frey, H. et al. Estimating the volume of glaciers in the Himalayan–Karakoram region using different methods. *Cryosphere* **8**, 2313–2333 (2014).
30. Huss, M. & Farinotti, D. Distributed ice thickness and volume of all glaciers around the globe. *J. Geophys. Res.* **117**, F04010 (2012).
31. Farinotti, D. et al. How accurate are estimates of glacier ice thickness? Results from ITMIX, the Ice Thickness Models Intercomparison eXperiment. *Cryosphere* **11**, 949–970 (2017).
32. Fürst, J. J. et al. Application of a two-step approach for mapping ice thickness to various glacier types on Svalbard. *Cryosphere* **11**, 2003–2032 (2017).
33. Maussion, F. et al. The Open Global Glacier Model (OGGM)v1.0. *Geosci. Model Develop. Discuss.* **2018**, 1–33 (2018).
34. Ramsankaran, R., Pandit, A. & Azam, M. Spatially distributed ice-thickness modelling for Chhota Shigri Glacier in western Himalayas, India. *Int. J. Remote. Sens.* **39**, 3320–3343 (2018).
35. RGI Consortium *Randolph Glacier Inventory—A Dataset of Global Glacier Outlines: Version 6.0* (Global Land Ice Measurements from Space (GLIMS), 2017).
36. Herman, F., Beaud, F., Champagnac, J.-D., Lemieux, J.-M. & Sternai, P. Glacial hydrology and erosion patterns: a mechanism for carving glacial valleys. *Earth Planet. Sci. Lett.* **310**, 498–508 (2011).
37. Haeberli, W. & Linsbauer, A. Global glacier volumes and sea level—small but systematic effects of ice below the surface of the ocean and of new local lakes on land. *Cryosphere* **7**, 817–821 (2013).
38. Immerzeel, W. W. & Bierkens, M. F. P. Asia's water balance. *Nat. Geosci.* **5**, 841–842 (2012).
39. Depoorter, M. A. et al. Calving fluxes and basal melt rates of Antarctic ice shelves. *Nature* **502**, 89–92 (2013).
40. Rignot, E. et al. Accelerated ice discharge from the Antarctic Peninsula following the collapse of Larsen B ice shelf. *Geophys. Res. Lett.* **31**, L18401 (2004).

41. Fürst, J. et al. The safety band of Antarctic ice shelves. *Nat. Clim. Change* **6**, 479–482 (2016).
42. Tachikawa, T., Hato, M., Kaku, M. & Iwasaki, A. Characteristics of ASTER GDEM version 2. In *Proc. IEEE Int. Geosci. Remote Sensing Symp. (IGARSS) 2011* 3657–3660 (IEEE, 2011).
43. Liu, H, Jezek, K, Li, B. & Zhao, Z. *Radarsat Antarctic Mapping Project Digital Elevation Model, Version 2* (NASA National Snow and Ice Data Center Distributed Active Archive Center, 2015).
44. Bahr, D. B., Pfeffer, W. T. & Kaser, G. Glacier volume estimation as an ill-posed inversion. *J. Glaciol.* **60**, 922934 (2014).

Acknowledgements

The contribution from J.J.F. was supported by the German Research Foundation (DFG grant no. FU1032/1-1), with numerical simulations facilitated by the high-performance computing centre at the University of Erlangen-Nuremberg (Regionales Rechenzentrum Erlangen (RRZE)). The support form R. Ramsankaran's research team at the Indian Institute of Technology Bombay is acknowledged. We thank the International Association of Cryospheric Sciences (IACS), co-chairs L. M. Andreassen and H. Li, and the members of the IACS Working Group on Glacier Ice Thickness Estimation for the support during the work. The analyses were performed in the frame of the Working Group's Global Glacier Thickness Initiative (G2TI).

Author contributions

D.F. conceived the study, performed the analyses of the results and drafted the manuscript, to which all the authors contributed. M.H., J.L. and D.F. prepared the necessary input data. M.H., J.J.F., H.M., F.M. and A.P. performed the calculations with individual models. M.H. and D.F. performed the GloGEM and Antarctic ice-discharge calculations, respectively.

Competing interests

The authors declare no competing interests.

Additional information

Supplementary information is available for this paper at https://doi.org/10.1038/s41561-019-0300-3.

Reprints and permissions information is available at www.nature.com/reprints.

Correspondence and requests for materials should be addressed to D.F.

Publisher's note: Springer Nature remains neutral with regard to jurisdictional claims in published maps and institutional affiliations.

Methods

Glacier morphology and measured ice thickness. All ice thickness estimates refer to the outlines provided through the RGI version 6.0 (ref. [35]). For every glacier (215,547 entities in total), the surface topography was extracted from either the hole-filled Shuttle Radar Topography Mission (SRTM) DEM version 4 (latitudes between 60° N and 60° S (ref. [45])), the ASTER Global DEM version 2 (ref. [42]) and the RAMP DEM version 2 (ref. [46]) (south of 60° S), or the Arctic DEM version 2.0 (north of 60° N (ref. [47])). Regions affected by data voids in the Arctic DEM were replaced by DEM3 (ref. [48]). To reduce the computational demand and depending on glacier size, the DEMs were resampled to a resolution of 25, 50, 100 or 200 m. The measured ice thickness was obtained from the GlaThiDa version 2.0 (ref. [13]), which provides ice thickness information for 1,085 glaciers.

Ice thickness estimates. The ice thickness of individual glaciers was estimated by using the above information and up to five different models. Ordered by the glacier area for which a solution was provided (Fig. 1), the models included those by Huss and Farinotti[30] (Model 1), Frey et al.[29] (Model 2), Maussion et al.[33] (Model 3), Fürst et al.[32] (Model 4) and Ramsankaran et al.[34] (Model 5). These models are capable of inverting for glacier ice thickness distributions at the mountain range scale. All the models infer the ice thickness distribution from surface characteristics (such as elevation and slope), an estimate of the glacier mass turnover and principles of ice flow dynamics. A summary description of the five models is given in Farinotti e al.[31], and Supplementary Section 1 and the original publications provide the details. For the ice thickness distribution of Svalbard, the area covered by the recent estimate of Fürst et al.[49] is replaced with that estimate. The remaining area is treated in the same way as the other regions. Fürst et al.[49] is based on Model 4, but used an additional set of more than 900,000 in situ ice thickness measurements that are not yet included in GlaThiDa. This provided substantially better model constraints than available within this study. Supplementary Figs. 6–24 provide examples for the ice thickness distribution generated by the individual models for selected glaciers (one per RGI region). Note that not all of the models provided an estimate for all of the RGI entries (Fig. 1), mainly because the requirements for manual interactions or the computational cost were unaffordable for the global-scale application.

Model weighting and uncertainty estimates. The final results are based on a composite solution $\hat{\mu}$ derived on a glacier-by-glacier basis through inverse variance and bias weighting[50]. For any given location, and assuming independence between the local ice thickness estimates h_i provided by the $n \leq 5$ models i, $\hat{\mu}$ is computed as:

$$\hat{\mu} = \frac{\sum h_i w_i^{-1}}{\sum w_i^{-1}} \quad (1)$$

where $w_i = |b_i| + \sigma_i^2$ is a weighting that reflects both the bias b_i and the variance σ_i^2 of the result produced by model i ($|b_i|$ denotes the absolute value of b_i and ensures that both over- and underestimates are penalized). To estimate b_i and σ_i^2, a cross-validation experiment was performed in which one-third of the available ice thickness measurements was randomly selected and used for model calibration, with the remaining two-thirds used for model validation. The experiment was repeated three times, and the deviations between modelled and measured ice thicknesses were expressed relatively to the mean ice thickness $\bar{h}$. The so-obtained deviations were pooled across the three experiments, and the mean and interquartile range of the pool were taken as an estimate for $b_i / \bar{h}_i$ and $1.5\sigma_i / \bar{h}_i$, respectively. The results of the cross validation are shown in Supplementary Fig. 1 and yielded relative weights of 22%, 19%, 18%, 28% and 13% for Models 1–5, respectively (last row of Supplementary Table 1). With the above notation, the variance of $\hat{\mu}$ is given by:

$$\sigma_{\hat{\mu}}^2 = \frac{1}{\sum \sigma_i^{-2}} \quad (2)$$

which is the basis for the presented accuracy estimates. Although we assume independence between the results obtained for a given glacier from different models, the results for different glaciers are assumed to be strongly correlated when they originate from the same model (or from the composite solution). When calculating regional totals, the uncertainties estimated for individual glaciers are thus summed. To assess the sensitivity of the above weighting strategy, regionally differentiated weights were tested as well. In that case, the weights in equation (1) were calculated by pooling the results of the cross-validation experiment separately for every RGI region (upper part of Supplementary Table 1). The results are insensitive (differences below 1%) to this alternative weighting scheme (Supplementary Table 3).

Sea-level change equivalents. The conversion between total glacier ice volume V_{tot} and potential sea-level change h_{SLE} was performed by (1) assuming a bulk ice density of $\rho_{ice} = 900\,kg\,m^{-3}$, an ocean area of $A_{ocean} = 3.625 \times 10^8\,km^2$ and a mean ocean density of $\rho_{ocean} = 1{,}028\,kg\,m^{-3}$ (ref. [51]), (2) neglecting the steric and isostatic effects and (3) subtracting glacier volumes V_{BSL} presently located below sea level:

$$h_{SLE} = \frac{V_{tot} - V_{BSL}}{A_{ocean}} \frac{\rho_{ice}}{\rho_{ocean}} \quad (3)$$

Future projections for High Mountain Asia. Reconstruction for the past (1998–2016) and projections for the future (2017–2100) glacier evolution and corresponding glacier runoff were obtained by forcing the GloGEM[10] with climate reanalysis data[52] and outputs from 14 different global climate models[53] driven by Representative Concentration Pathway 4.5 (a midrange scenario for future climate evolution[54]), respectively. The model calibration, parameter choice and downscaling of climate model outputs are identical to those in Huss and Hock[10]. Two different simulations were performed for the time period 1998–2100, the only difference being the ice thickness distribution used to initialize the model. The model provides the glacier area (with an annual time step) and glacier runoff (with a monthly time step) of every glacier individually, and the results are aggregated over RGI regions 13, 14 and 15 (Table 1 and Fig. 2). Uncertainties due to unknown future climate evolution are taken into account through the output of different climate models. Further uncertainties are not accounted for explicitly as they have been shown to be comparatively small[10].

Ice discharge from Antarctic glaciers. Ice discharge estimates for glaciers in the Antarctic periphery are based on surface ice flow velocities provided in Rignot et al.[55]. For every glacier, the calving front was identified by selecting portions of the glacier outline that have a bedrock located below present-day sea level (roughly 250 of the 2,751 glaciers in the region are detected to have such a calving front). The volumetric ice discharge was then obtained by multiplying the local, depth-averaged ice flow velocity with the local ice thickness and by integrating the so-obtained values over the calving front length. Uncertainties in surface velocities are provided within the data set[55], whereas uncertainties in depth-averaged values are estimated by considering two end members: the first assumes that the entire surface motion is due to basal sliding (plug flow), and the second assumes the surface velocity is entirely due to ice deformation. The reported results refer to the average of the two end members. A bulk density of $900\,kg\,m^{-3}$ was used to convert ice volume flux to mass flux.

Code availability

The codes used to generate individual results are available through the contact information from the original publications. Requests for further materials should be directed to D.F.

Data availability

The ice thickness distribution of all about 215,000 glaciers, as estimated with the individual models and the composite solution, is available at https://doi.org/10.3929/ethz-b-000315707.

References

45. Jarvis, J., Reuter, H., Nelson, A. & Guevara, E. *Hole-Filled SRTM for the Globe Version 4* (CGIAR Consortium for Spatial Information, 2008).
46. Liu, S. et al. Glacier retreat as a result of climate warming and increased precipitation in the Tarim river basin, northwest China. *Ann. Glaciol.* **43**, 91–96 (2006).
47. Porter, C. et al. ArcticDEM V1 (Harvard Dataverse, 2017); https://doi.org/10.7910/DVN/OHHUKH
48. de Ferranti, J. A *Worldwide 3 Arc Seconds DEM* (2014); http://viewfinderpanoramas.org/dem3.html
49. Fürst, J. et al. The ice-free topography of Svalbard. *Geophys. Res. Lett.* **45**, 760–711 (2018).
50. Hartung, J., Knapp, G. & Sinha, B. *Statistical Meta-analysis with Applications* (John Wiley & Sons, Hoboken, 2008).
51. Conkright, M. et al. *World Ocean Atlas 2001: Objective Analyses, Data Statistics, and Figures, CD-ROM Documentation* 17 (National Oceanographic Data Center, Silver Spring, 2002).
52. Dee, D. et al. The ERA-Interim reanalysis: configuration and performance of the data assimilation system. *Q. J. R. Meteorol. Soc* **137**, 553–597 (2011).
53. Taylor, K., Stouffer, R. & Meehl, G. An overview of CMIP5 and the experiment design. *Bull. Am. Meteorol. Soc.* **93**, 485–498 (2012).
54. Meinshausen, M. et al. The RCP greenhouse gas concentrations and their extensions from 1765 to 2300. *Climatic Change* **109**, 213–241 (2011).
55. Rignot, E, Mouginot, J. & Scheuchl, B. *MEaSUREs InSAR-Based Antarctica Ice Velocity Map, Version 2* (NASA National Snow and Ice Data Center Distributed Active Archive Center, 2017).